JOURNAL OF GEOPHYSICAL RESEARCH, VOL. 106, NO. D11, PAGES 11,967–11,976, JUNE 16, 2000

Ground measurements of surface BRF and HDRF using PARABOLA III

Wedad A. Abdou, Mark C. Helmlinger, James E. Conel, Carol J. Bruegge, Stuart H. Pilorz, John V. Martonchik, and Barbara J. Gaitley

Jet Propulsion Laboratory, California Institute of Technology, Pasadena, California

Abstract. The ground-based Portable Apparatus for Rapid Acquisition of Bidirectional Observations of Land and Atmosphere (PARABOLA), version 3, provides multiangle measurements of sky and ground radiances on a spherical grid of 5° in the zenith-to-nadir and azimuthal planes in eight spectral channels. The hemispherical directional reflectance factor (HDRF) can be measured directly by comparing the radiance reflected by the surface in given direction to that reflected from a reference surface simultaneously observed by the PARABOLA 3. The surface bidirectional reflectance factor (BRF) cannot be measured directly, however, because of the presence of the sky diffuse illumination. The contribution of the diffuse sky radiance to the radiance reflected by the natural target surface is computed, and removed, using an iterative technique. Two approaches are employed: the first requires knowledge of the atmospheric optical depth, and the second requires the simultaneous measurements of the radiance reflected by a standard surface panel under the same atmospheric and illumination conditions. Ground measurements of the BRF and HDRF for dry lake surfaces were obtained from the PARABOLA 3 observations with better than ±10% accuracy. The results described in this work are used primarily for the vicarious calibration of the Multiangle Imaging Spectroradiometer (MISR) onboard the Earth Observing System (EOS) Terra platform and for validation of MISR BRF retrievals of selected Earth surface targets.

1. Introduction

Surface-atmosphere radiative coupling is dominated by the reflectance properties of the surface. All natural surfaces exhibit anisotropic reflection which is described by the bidirectional reflectance factor (BRF) and the hemispherical directional reflectance factor (HDRF). Knowledge of the surface BRF, on global scale, is crucial to the assessment of the Earth radiation budget and to the ongoing research effort on climate and global changes [e.g., *Dickinson et al*., 1990; *Mintz*, 1984; *Charney et al*., 1977]. Theoretical models have been developed to calculate the surface BRF [e.g., *Liang and Strahler*, 1993; *Verstraete et al*., 1990; *Pinty and Verstraete*, 1992; *Pinty et al*., 1989] using a number of parameters to provide the physical and optical properties of the surface.

Estimates of the surface directional reflectance properties, on global and regional scales, can best be achieved using observations of spaceborne and airborne multiangle spectroradiometers, such as the multiangle imaging spectroradiometer (MISR) [*Diner et al*., 1998a] and its airborne simulator AirMISR [*Diner et al*., 1998b] and the airborne advanced solid-state array spectroradiometer (ASAS) [*Irons et al*., 1991], after applying the appropriate atmospheric correction algorithm to the observed top-of-atmosphere data [*Liang and Strahler*, 1994; *Martonchik et al*., 1998].

Ground measurements are required to support, supplement, and validate spaceborne and airborne observations. The Portable Apparatus for the Rapid Acquisition of Bidirectional Observations of Land and Atmosphere (PARABOLA 3) [*Bruegge et al*., 2000a] is a sphere-scanning radiometer that provides complete hemispherical measurements of sky and surface radiances in a 5° field of view and in eight spectral channels (444, 551, 650, 860, 944.0, 1028, 1650, and 400–700 nm). Ground measurements made with the PARABOLA 3 are used in this work to determine the BRF and HDRF functions for natural target surfaces. An earlier version that provides fewer angular observations, in a 15° field of view in three spectral bands, has also been described and used [*Deering*, 1988; *Deering and Leone*, 1986].

The PARABOLA 3 ground measurements described here are used primarily for the validation and vicarious calibration of MISR and AirMISR [*Abdou et al*., 2000]. MISR and AirMISR provide images of Earth at nadir and along-track angles of ±26°, ±45°, ±60°, and ±70° relative to nadir, in four bands (446, 558, 672, and 866 nm). Global characterization of the surface BRF, among other products, is produced from MISR observations. In this paper the PARABOLA 3 field measurements from three AirMISR vicarious calibration campaigns at Lunar Lake, Nevada, in June 1997, and at Rogers Lake, California, in May and December 1998, are presented, and the techniques used to process the data and retrieve the surface BRF and HDRF are described.

2. Definitions of the Surface Directional Reflectance Properties

There are several reflectance functions that are commonly used by the remote sensing community to describe the directional reflectance properties of a surface. Complete definitions of these functions are given by *Nicodemus et al*. [1977], *O'Neill et al*. [1995], and *Bruegge et al*. [2000b]. Two of these, relevant to the present work, are briefly defined here.

Paper number 2000JD900654.
0148-0227/01/2000JD900654$09.00

2.1. Bidirectional Reflectance Factor

The BRF is an inherent property of the surface, defined as the ratio of the radiance L_t^r reflected by the target surface in a specific direction to that reflected in the same direction by a perfect diffuse (Lambertian) surface under the same parallel beam illumination. Since the radiance reflected by a perfect (nonabsorbing) Lambertian surface is uniformly distributed and is equal to $1/\pi$ of the incident irradiance E^i, then the BRF, R, is given as

$$R(\lambda, -\mu, \varphi, \mu_0, \varphi_0) = \frac{L_t^r(\lambda, -\mu, \varphi, \mu_0, \varphi_0)}{(1/\pi)E^i(\lambda, \mu_0, \varphi_0)}, \quad (1)$$

where, λ is the wavelength, μ_0 and μ are, respectively, the direction cosines of the zenith angles, θ_0 and θ, of the incident and reflected radiances, measured with respect to the normal to the surface (the negative sign indicating upward direction), and ϕ_0 and ϕ are, respectively, the azimuth angles of the incident and reflected radiances.

2.2. Hemispherical Directional Reflectance Factor

The HDRF r is defined as the ratio of the radiance reflected by the surface in a specific direction to that reflected, in the same direction, by a perfect Lambertian surface under the same ambient illumination. Therefore

$$r(\lambda, -\mu, \varphi, \mu_0, \varphi_0) = \frac{\frac{1}{\pi}\int_0^1\int_0^{2\pi} R(\lambda, -\mu, \varphi, \mu', \varphi')}{\frac{1}{\pi}\int_0^1\int_0^{2\pi} L^i(\lambda, \mu', \varphi', \mu_0, \varphi_0)\mu'\, d\mu'\, d\varphi'} = \frac{L^i(\lambda, \mu', \varphi', \mu_0, \varphi_0)\mu'\, d\mu'\, d\varphi'}{\int_0^1\int_0^{2\pi} L^i(\lambda, \mu', \varphi', \mu_0, \varphi_0)\mu'\, d\mu'\, d\varphi'}, \quad (2)$$

where L^i, the radiance incident on the surface, includes both direct (parallel) and diffuse illumination. The HDRF is not an inherent property of the surface but varies according to the ambient illumination.

Radiative transfer studies usually require knowledge of the surface BRF to account for the surface-atmosphere radiative coupling. However, from the above definitions, and as will be shown later, direct field measurements of the surface HDRF are much simpler to obtain than those of the BRF. Therefore knowledge of the HDRF can be valuable in case of clear-sky conditions, where the ratio of direct solar to hemispherical irradiance can be more than 10 to 1 and the surface HDRF is a very good approximation of the surface BRF.

3. PARABOLA 3 Field Experiment and Data Processing

The PARABOLA (herein the "3" referring to the instrument version, used at the Jet Propulsion Laboratory, will be omitted for convenience) provides complete hemispherical scans of the sky downwelling and surface upwelling radiances, on a 5° spherical grid, in eight spectral channels at 444, 551, 650, 860, 944, 1028, 1650, and 400–700 nm. The first four of these channels nearly coincide with four MISR channels, both in center wavelength and band pass, and are used for validation and vicarious calibration of MISR and AirMISR. The latter four channels are used for evaluating water vapor, aerosol optical depth at longer wavelength, and measurements of photosynthetically active radiation (PAR). A detailed description of the PARABOLA, its calibration and performance in the field, are presented by *Bruegge et al*. [2000a]. In this work, emphasis is on how the field observations are processed and used to determine the surface BRF and HDRF.

In the field, PARABOLA is normally set about 2 m above the ground. The instrument is leveled horizontally such that the elevation of each of the eight sensor heads is aligned 180° with respect to nadir. From this initial position the PARABOLA observations start by scanning the sky, in 5° steps in the azimuthal plane, beginning from an arbitrary reference azimuth. These azimuthal scans are repeated 36 times as the elevations of the sensor heads decrease, in 5° steps, from 180° to 0°. The complete spherical scan is concluded by scanning the ground with the sensor heads looking in the nadir. Illustrations of sky and ground projections of the PARABOLA field of view are given by *Bruegge et al*. [2000a]. At the end of each spherical scan, the sensor heads return to the starting position and the data are written to a file by the instrument computer. A complete spherical scan takes ~3 min and represents one data record consisting of 37×72 values of instrument response per channel, 37 elevation angles, and 72 azimuthal angles, and the time (in UT). The latter is usually recorded at the beginning of each scan.

A Spectralon panel, 25 cm on a side, is placed under the sensor heads, and on the south side of their trajectory to remain illuminated for the entire period of the measurements. This allows direct determination of the surface HDRF from PARABOLA observations. The radiance reflected by the Spectralon surface is measured at nadir and from 5° to 15° off nadir. Spectralon is a diffuse reflector commonly used as a bright reference standard for reflectance measurements. In practice, the Spectralon reflectance deviates slightly from that of a perfect Lambertian surface, and a correction factor equal to the Spectralon BRF is required to correct for its nonideal reflectance properties. The BRF of the Spectralon panel was measured in the laboratory as described by C. J. Bruegge et al. (A Spectralon BRF database for MISR calibration applications, submitted to *Remote Sensing Environment*, 2000c) (hereinafter referred to as B2000).

3.1. Data Processing

Figure 1 illustrates the unprocessed data from one of the PARABOLA spherical scans over Rogers Dry Lake, on May 10, 1998. Four major steps are required to prepare the PARABOLA data for the evaluation of the HDRF and the BRF.

3.1.1. Correction of azimuth and zenith angles. The field observations are measured in the azimuth plane with respect to an arbitrary reference direction. The Sun elevation, as determined by the PARABOLA, is correct only within the instrument field of view, i.e., to $\sim\pm5°$. The observations are referenced to the Sun ephemeris using least squares fit. Figure 2 compares the solar ephemeris at Rogers Lake, California, on May 10, 1998, to the Sun positions, as determined by the PARABOLA before and after corrections. As shown in this figure, except for a few cases, the agreements between the true and the corrected Sun angle are better than $\pm1°$.

3.1.2. Locating the Spectralon panel. The data points corresponding to the Spectralon-reflected radiances (seen in bottom left corner of Figure 1) are located, removed, and saved for later use in the retrieval of the surface parameters. These data are then replaced by values representative of the

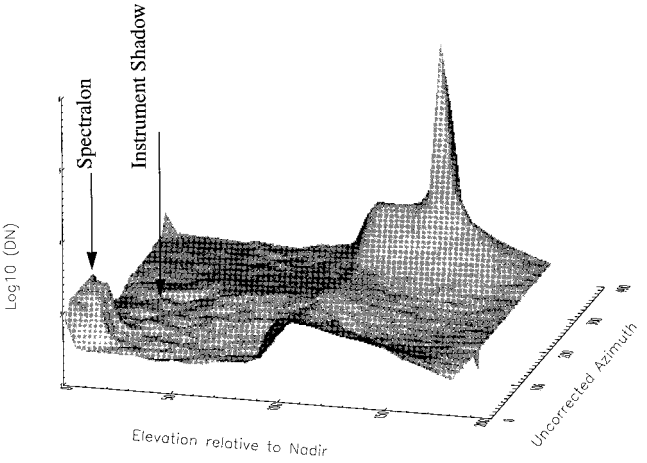

Figure 1. Illustration of a PARABOLA scan at Rogers Lake, May 10, 1998, at 1600 UT. The unprocessed data represent the instrument response (DN) at 551 nm to the downwelling sky-radiance (right-hand side of the plot) and the upwelling surface-reflected radiance (left-hand side) as a function of the view angles. The latter are measured along the look direction by the PARABOLA internal compass. The peak represents the instrument response to radiance coming directly from the Sun which, at 1600 UT, is at elevation of ~127° and at 93.5° with respect to the geographic North.

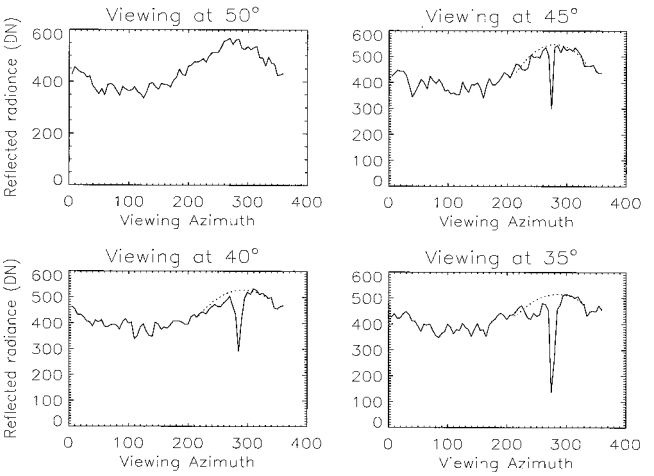

Figure 3. A sample of the data in Figure 1 to illustrate instrument shadows and their corrections. The view angles (along the look direction) are corrected according to the solar ephemeris. The instrument shadow appears at view zenith angle of 45° and view azimuth angle of ~275°, i.e., 180° from the Sun azimuth angle. The data near the shadow are corrected by interpolation and curve fitting to preserve the backward scattering and/or the hot spot.

surface-reflected radiances, by interpolating observations along the azimuth direction.

3.1.3. Shadow corrections. The PARABOLA is usually set in the field away from buildings or any large structures. The instrument shadow, however, always appears in the hemispherical scanning of the surface, as shown in Figure 1, at view zenith angles equal to or less than the Sun zenith angle and centered at azimuth angle 180° from the Sun. Because consecutive observations overlap in the azimuthal direction, the shadow usually dominates a range of data points along that direction, as shown in Figure 3. An automated shadow correction procedure locates the center of the instrument shadow and determines its range along the azimuthal direction. The data within this range is replaced by interpolating and curve fitting the data outside and on both sides of the shadow range, as illustrated by the dotted line in Figure 3.

3.1.4. Restoring the hot spot. The hot spot can be observed in the principal plane in the reverse solar direction. Hot spots are usually totally or partially masked by the shadow of the instrument. However, one can detect the presence of a hot spot by carefully examining the data near the edge of the shadows and, if any exists, the shadow correction procedure, described above, automatically restores it. This is an approximate procedure. However, detailed analysis of the hot spot is not part of the present work. Figure 4 shows the data of Figure 1, after all the above corrections were applied.

3.1.5. Radiometric calibration. The PARABOLA digital responses, DN, are converted into radiances according to the following relation:

$$DN_n - DN_{0,n} = g_{0,n} + g_{1,n}L_n + g_{2,n}L_n^2, \quad (3)$$

where DN_0 is the dark current, g_0 is the offset, and g_1 and g_2 are the gain coefficients for the nth channel and were deter-

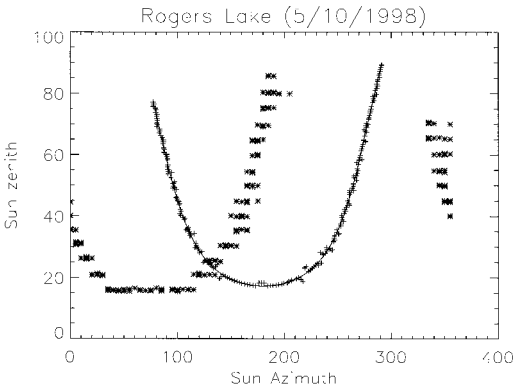

Figure 2. Solar ephemeris (the solid line) at Rogers Lake, California (34.97° latitude and −117.83° longitude), on May 10, 1998. The Sun position as measured by the PARABOLA, before and after correction (see section 3.1.1) are represented by the asterisks and the pluses, respectively.

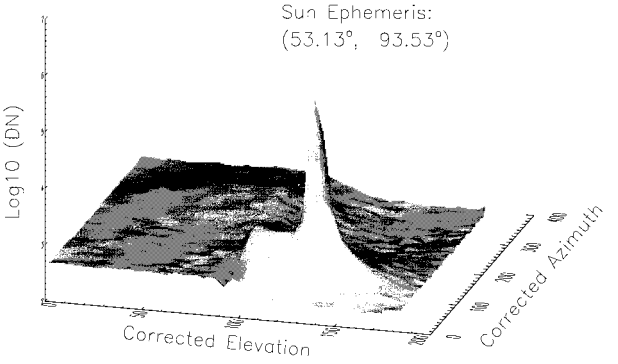

Figure 4. PARABOLA scan, shown in Figure 1, after all corrections described in 3.1 are applied. The view angles are along the look direction.

mined in the laboratory for each of the PARABOLA channels [*Bruegge et al.*, 2000a]; g_2 is usually very small ($10^{-4} < g_2 < 4 \times 10^{-2}$) and, to a very good approximation, can be ignored.

3.2. Auxiliary Data

Because the PARABOLA is used primarily for validation and vicarious calibration of MISR and AirMISR, other instruments are simultaneously used to collect additional observations. These instruments include one or two solar radiometers to measure the atmospheric optical depth, and a portable spectrometer, manufactured by analytical spectral devices (ASDs), which allows a rapid estimation of the surface spectral HDRF in the nadir direction between 350 and 2500 nm. The ASD instrument has been traditionally used to calibrate nadir-viewing sensors and, in this work, to validate the PARABOLA observations near nadir. The ASD observations of the radiance reflected by the natural target surface and the Spectralon standard surface are obtained in a sequential and fast manner within ±1 hour of solar noon when the change in Sun elevation is smallest. The nadir-viewing HDRF of the target surface is given by

$$r_{t(\mathrm{ASD})}(\lambda, -1, \mu_0, \varphi_0) = \frac{V_t(\lambda, \mu_0) - V_0(\lambda, \mu_0)}{V_{\mathrm{spect}}(\lambda, \mu_0) - V_0(\lambda, \mu_0)} r_{\mathrm{spect}}(\lambda, -1, \mu_0, \varphi_0), \quad (4)$$

where V_0 is the dark current, and V_t and V_{spect} are the ASD responses to the target and standard surfaces, respectively. The -1 refers to zero view angle in the upward direction. The Spectralon HDRF, r_{spect}, is needed to correct for the nonideal Lambertian properties of the Spectralon, as is explained in section 4.1.

The PARABOLA experiment is conducted under clear sky and atmospheric conditions so that short-term fluctuations in illuminating geometry during the PARABOLA scans are negligible. Also, the surface is chosen to be spatially homogeneous with surface properties varying minimally (usually less than 1% in reflectance over the entire experiment site, so observations of both the PARABOLA and the ASD represent the same average characteristics of the target.

4. Methods of Retrieving Surface Properties from PARABOLA Observations

4.1. HDRF Retrieval

From each PARABOLA spherical scan, the surface HDRF can be directly determined for the atmospheric conditions and illumination angles specific to the time of that scan. The HDRF, given by equation (2) can also be expressed as

$$r_t(-\mu, \mu_0, \phi - \varphi_0) = \frac{L_t^r(-\mu, \mu_0, \phi - \varphi_0)}{L_{st}^r(\mu_0)}, \quad (5)$$

where L_t^r and L_{st}^r refer to the radiances reflected by the target and the standard perfect Lambertian surfaces, respectively, and where it is assumed that the azimuth dependence of the reflected radiance is a function of $\phi - \phi_0$ only. For simplicity of notation the spectral dependency is omitted. Since the standard surface has a perfect Lambertian reflectance, L_{st}^r is independent of μ and $\phi - \phi_0$. However, the reflectance properties of the Spectralon, used in this work as the standard surface, deviates slightly from a perfect Lambertian. Since the HDRF for Spectralon can also be expressed in a form like (5) then

$$r_{\mathrm{Spect}}(-1, \mu_0) = \frac{L_{\mathrm{spect}}^r(-1, \mu_0)}{L_{st}^r(\mu_0)}, \quad (6)$$

and r_t can be written as

$$r_t(-\mu, \mu_0, \phi - \varphi_0) = \frac{L_t^r(-\mu, \mu_0, \phi - \varphi_0)}{L_{\mathrm{Spect}}^r(-1, \mu_0)} \times r_{\mathrm{Spect}}(-1, \mu_0). \quad (7)$$

Therefore to evaluate the HDRF of the target surface in any direction from the PARABOLA data, knowledge of the Spectralon HDRF in the nadir is required. A Spectralon BRF database (B2000) was substituted for the HDRF after conducting a sensitivity study to evaluate the expected errors. The errors were evaluated at all PARABOLA wavelengths, for a range of solar zenith angles up to 75° and for two atmospheric conditions, one clear with a visibility of >100 km and the other relatively hazy with a visibility of ~20 km. The results show that the errors in using the Spectralon BRF in (7), instead of the HDRF, generally increase with solar zenith angle, decrease with wavelengths, and are larger for hazy atmospheric conditions. For clear atmospheric conditions, the errors are always <1% for all solar angles up to 75°. For the hazy conditions, these errors are <1% up to solar angles of 50° for all of the PARABOLA bands, increasing to a maximum of 1% for larger Sun angles at all wavelengths above 550 nm and to ~2.5% at 450.0 nm. Generally, such errors are insignificant except at short wavelengths under hazy atmospheric conditions.

Replacing radiance by instrument DN and the Spectralon HDRF by its BRF, (7) becomes

$$r_t(-\mu, \varphi, \mu_0, \varphi_0) = \frac{DN_t^r(-\mu, \varphi, \mu_0, \varphi_0) - g_0}{DN_{\mathrm{Spect}}^r(-1, \mu_0) - g_0} \times R_{\mathrm{Spect}}(-1, \mu_0). \quad (8)$$

Presently, the dark currents are not subtracted from the instrument DNs because they were not included in the laboratory determination of g_0 [*Bruegge et al.*, 2000a] and thus far have not been determined in the field. Ideally, there should be good agreement between the ASD and the PARABOLA measurements of the HDRF in the nadir. To minimize errors due to this dark current issue, the nadir HDRF measured by the ASD is substituted for r_t to evaluate g_0 from (8). Errors in the values of g_0 determined with this approach are estimated to be within 1.5%.

4.2. BRF Retrieval

Since the PARABOLA field observations include the diffuse component of the incident and reflected radiances, a determination of the BRF from the PARABOLA or any PARABOLA-like observations must include removing the diffuse component. This is achieved using an iterative algorithm developed by *Martonchik* [1994]. The algorithm is employed in this work using two approaches: (1) the absolute-radiance approach, based on an estimation of the absolute value of the radiance reflected directly by the target surface, and (2) the relative-radiance approach, based on the estimation of the radiance reflected directly by the target surface relative to that reflected directly by the Spectralon panel. The following describes these two approaches in detail:

4.2.1. The absolute-radiance approach. This approach utilizes (1), which can be rewritten as follows:

$$R_t(-\mu,\ \mu_0,\ \varphi-\varphi_0) = \frac{L_t^r(-\mu,\ \mu_0,\ \varphi-\varphi_0) - L_t^{r(\mathrm{diff})}(-\mu,\ \mu_0,\ \varphi-\varphi_0)}{\left(\frac{1}{\pi}\right)\mu_0 E_0 e^{-\tau/\mu_0}}, \quad (9)$$

where E_0 is the band-averaged exoatmospheric irradiance, and τ is the atmospheric optical depth. L_t^r is the radiance reflected by the target surface, and $L_t^{r(\mathrm{diff})}$ is its diffuse component, given by

$$L_t^{r(\mathrm{diff})}(-\mu,\ \mu_0,\ \varphi-\varphi_0) = \frac{1}{\pi}\int_0^1\int_0^{2\pi} R_t(-\mu,\ \mu',\ \varphi - \varphi')L^{i(\mathrm{diff})}(\mu',\ \mu_0,\ \varphi'-\varphi_0)\mu'\,d\mu'\,d\varphi', \quad (10)$$

where $L^{i(\mathrm{diff})}$ is the diffuse incident radiance. In (9) and (10), L_t^r and $L^{i(\mathrm{diff})}$ are measured by PARABOLA.

This approach therefore requires knowledge of the exoatmospheric solar irradiance and the atmospheric optical depth. The first is acquired from a database [*Wehrli*, 1986], and the second is simultaneously measured in the field by a solar radiometer. The PARABOLA digital responses are converted into radiances using (3), before using them in these calculations. It is important to note that to evaluate $L_t^{r(\mathrm{diff})}(-\mu,\ \mu_0,\ \varphi-\varphi_0)$, the direct Sun must be removed from the incident radiance observed by the PARABOLA.

The iteration process starts using a first estimate $R_t^{(1)}$ for the BRF. This can be obtained by initially assuming that (1) $R_t^{(1)} = r_t$, to calculate the first iteration of $L_t^{r(\mathrm{diff})(1)}(-\mu,\ \mu_0,\ \varphi-\varphi_0)$ from equation 10, or (2) $L_t^{r(\mathrm{diff})(0)}(-\mu,\ \mu_0,\ \varphi-\varphi_0) = 0$, and calculate the first estimate of R_t from (9), using the upwelling radiances measured by PARABOLA. These two initial assumptions produce results within 1% of each other. The nth estimate of the BRF is then given by

$$R_t^{(n)}(-\mu,\ \mu_0,\ \varphi-\varphi_0) = \frac{L_t^r(-\mu,\ \mu_0,\ \varphi-\varphi_0) - L_t^{r(\mathrm{diff})(n-1)}(-\mu,\ \mu_0,\ \varphi-\varphi_0)}{\left(\frac{1}{\pi}\right)\mu_0 E_0 e^{-\tau/\mu_0}}. \quad (11)$$

The iteration reaches convergence when the reflected radiance $\hat{L}_t^r$ estimated from the nth iteration; that is,

$$\hat{L}_t^r(-\mu,\ \mu_0,\ \varphi-\varphi_0) = \left(\frac{1}{\pi}\right)\mu_0 E_0 e^{-\tau/\mu_0} R_t^{(n)}(-\mu,\ \mu_0,\ \varphi-\varphi_0) + L_t^{r(\mathrm{diff})(n)}(-\mu,\ \mu_0,\ \varphi-\varphi_0) \quad (12)$$

is within a set limit of the PARABOLA observed value, i.e., when

$$\frac{L_t^r(-\mu,\ \mu_0,\ \varphi-\varphi_0) - \hat{L}_t^r(-\mu,\ \mu_0,\ \varphi-\varphi_0)}{L_t^r(-\mu,\ \mu_0,\ \varphi-\varphi_0)} \le \varepsilon. \quad (13)$$

Generally, this convergence criterion is achieved faster (within two to three iterations) for smaller Sun and viewing zenith. In this work, ε is set to 0.03.

4.2.2. The relative-radiance approach. This approach also utilizes (1), which in this case is rewritten as follows:

$$R_t(-\mu,\ \mu_0,\ \varphi-\varphi_0) = \frac{L_t^r(-\mu,\ \mu_0,\ \varphi-\varphi_0) - L_t^{r(\mathrm{diff})}(-\mu,\ \mu_0,\ \varphi-\varphi_0)}{L_{\mathrm{spect}}^r(-1,\ \mu_0) - L_{\mathrm{spect}}^{r(\mathrm{diff})}(-1,\ \mu_0)} \times R_{\mathrm{spect}}(-1,\ \mu_0) \quad (14)$$

where

$$L_{\mathrm{spect}}^{r(\mathrm{diff})}(-1,\ \mu_0) = \frac{1}{\pi}\int_0^1\int_0^{2\pi} R_{\mathrm{spect}}(-1,\ \mu')L^{i(\mathrm{diff})}(\mu',\ \mu_0,\ \varphi' - \varphi_0)\mu'\,d\mu'\,d\varphi'. \quad (15)$$

The denominator of (14) is evaluated once, using (15), the PARABOLA measurements of L_{spect}^r, $L^{i(\mathrm{diff})}$, and the values of R_{spect} from database. Equation (14) is clearly equivalent to (11), and $L_t^{r(\mathrm{diff})}$ is then evaluated using the same iterative algorithm described in 4.2.1.

The advantage of this approach over the absolute-radiance approach is that no data other than PARABOLA observations and the Spectralon BRF database are required. Also, in (14), because the radiance reflected by the target surface is related to that reflected by the Spectralon, the gain coefficient g_1 cancels out, eliminating a major source of error. Using the ASD data to estimate g_0, as explained above, helps reduce the remaining source of error.

5. Results

5.1. Site Description

PARABOLA data collected during three AirMISR vicarious calibration experiments were analyzed. The experiments were conducted at Lunar Lake, Nevada (38.39° latitude, and −115.99° longitude) in June 1997, and at Rogers Lake, California (34.97° latitude and −117.83° longitude), in May 1998 and in December 1998. The dry surfaces are essentially flat and level, so no correction for surface tilt is required in these cases. Rogers Lake is contained within Edwards Air Force Base, California, and is dry except for winter months, when standing water may be present for short periods. During dry conditions the silt size of surface material is a uniform, bright diffuse reflector largely free of loose material. Mud cracks are pervasive throughout the test area where contraction of the lake surface, upon drying from wet conditions, forms polygonal patterns of average dimension ~20 cm. Cracks give rise to shadowing on edges facing away from the Sun, and to brighter strips on opposite-facing edges. Lunar Lake is also subject to flooding during winter and early spring months. Evaporation of standing lake waters also produces polygonal, upward concave (saucer shaped) mud crack surfaces of the order of ~15 cm in dimension. Individual saucers display specular-like reflection, best seen at low Sun elevation angles. The specular reflectance is caused by accumulations of platy minerals at the surface that settle out of residual waters before evaporation is complete.

During the experiments, AirMISR overflew the site onboard one of the NASA ER-2 planes. On the ground the PARABOLA is usually set in the field early in the morning, and measurements are collected from sunrise to sunset. Simultaneously, the Sun photometer is used to measure the atmospheric optical depth at various times of the day. The nadir-

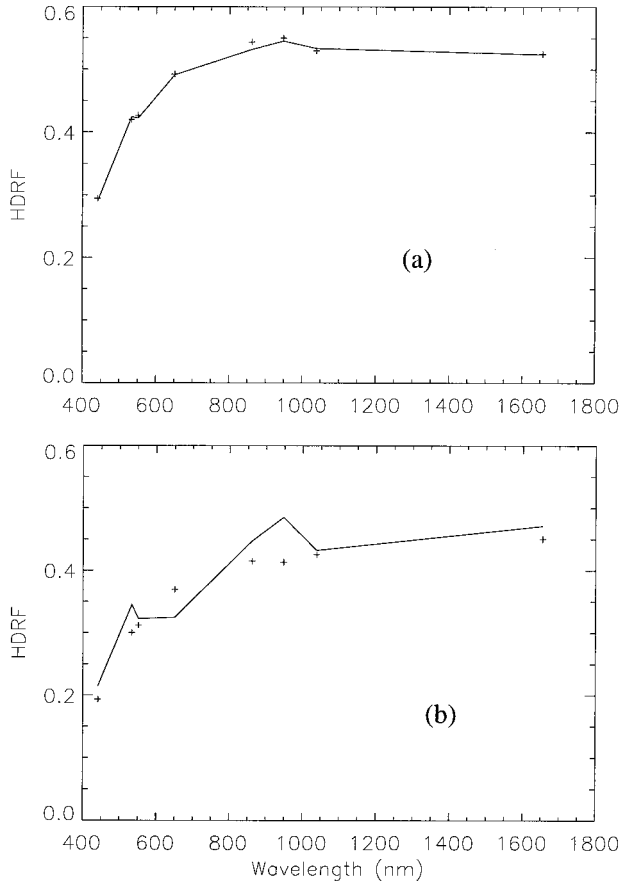

Figure 5. Nadir HDRF determined from the PARABOLA data (solid lines) and the ASD data (pluses) are shown in (a) Lunar Lake, Nevada, on June 24, 1997, and (b) for Rogers Lake, California, on May 10, 1998. The HDRF were calculated from the ASD using equation (4) and from the PARABOLA data using equation (8) and the laboratory measured g_0. The disagreement shown in Figure 5b indicates changes in the PARABOLA radiometric calibration.

viewing ASD instrument is operated within $\sim\pm1$ hour from the AirMISR overpass time, usually about 1100–1130 LT.

The experiment sites are located at high desert areas where the atmosphere is clean and visibility is typically >100 km. The measured atmospheric optical depths are usually small, ranging from 0.1–0.2 in the visible to less than 0.02 at 1650 nm. At Rogers Lake, on May 10, 1998, however, the optical thickness was ~0.2–0.4 in the visible to ~0.05 at 1650 nm. Only data collected during cloud-free sky conditions are used in the present analyses.

5.2. HDRF Results

The nadir-view HDRF using ASD observations was calculated using (4), substituting R_{spec} for r_{spec}, to correct for the nonideal Lambertian properties of the Spectralon. The surface HDRF was also calculated for the nadir view using the PARABOLA data and (8). The PARABOLA data in the nadir were averaged over all azimuth angles before using them in these calculations, and the ASD data were convolved spectrally to the PARABOLA passbands. The PARABOLA and the ASD results for the Lunar Lake campaign are in good agreement, within $\sim\pm1\%$, for most channels, as shown in Figure 5a. However, a year later at Rogers Lake campaign, this agreement deteriorated, as is illustrated by Figure 5b, indicating a change in the PARABOLA radiometric calibration. Based on this, corrected values for the offset factor g_0 were estimated, by substituting $r_{t(\text{ASD})}$ for the nadir viewing in (8) and were then used to calculate the HDRF from the PARABOLA observations for all viewing and illuminating geometries.

For the two summer campaigns at Lunar Lake and Rogers Lake, measurements were collected for a wide solar zenith angle range of ~18° at solar noon to >80° at dawn and dusk. In the winter campaign at Rogers Lake the zenith angle at solar noon was at 58°. The results are calculated for all available viewing and illuminating geometries, in every PARABOLA channel. Only a few samples are presented here to illustrate the main features of the surface HDRF at each campaign site. The plots in Figures 6a and 6b illustrate the surface HDRF at Lunar Lake at 550 nm for two illumination geometries. The results show a prominent forward scattering, eye witnessed in the field, which increases as the Sun moves toward the horizon. Opposite the Sun the surface appears more diffuse with a slight increase in backward scattering as the solar

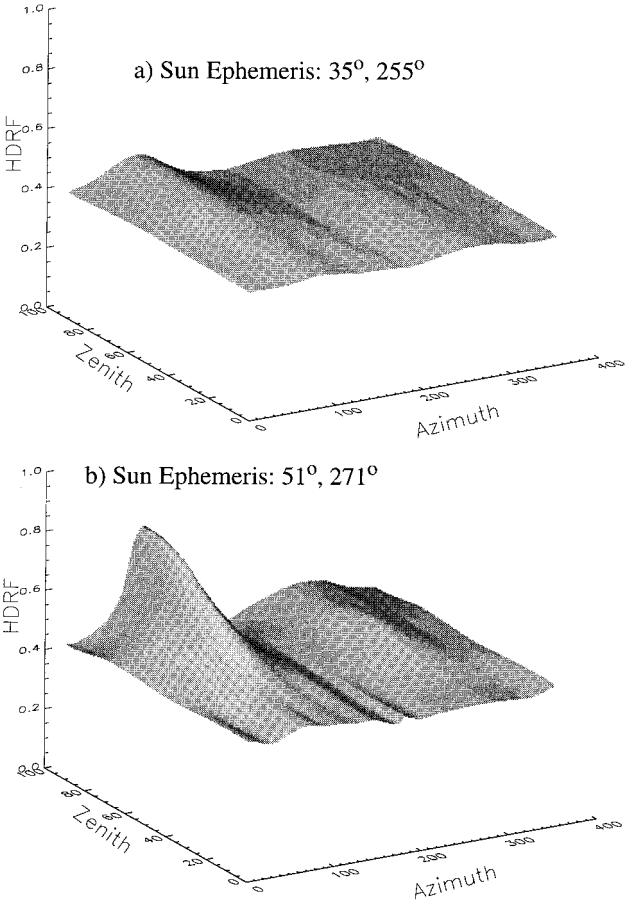

Figure 6. Samples of the surface HDRF results for Lunar Lake, Nevada, on June 24, 1997, for various illuminating and viewing geometries at 551 nm. The view zenith and azimuth angles are presented along the radiance direction. The solar ephemeris indicated on each figure represents the Sun position (in the look direction). The figures indicate a dominant forward scattering which increases as the Sun approaches the horizon. The shades of gray in this figure are automatically generated by the plotting routine and have no quantitative values.

zenith angle increases. The same characteristics are illustrated in Figure 7, where the HDRF from the Lunar Lake data set is presented in the principal plane as a function of the viewing zenith angles. Figure 7 shows the strong forward scattering ($\phi - \phi_0 = 0$) which maximizes at angles larger than the solar zenith angle. The backward scattering ($\phi - \phi_0 = 180$) is almost uniformly diffuse, with a slight bump (in some of the channels) at an angle close to the Sun zenith angle, indicating a weak hot spot.

At Rogers Lake the surface HDRF behaves very differently from that at Lunar Lake. As shown in Figure 8, both backward and forward scattering increase near-horizon viewing, with the backward scattering becoming increasingly prominent at larger solar angles. Near solar noon the surfaces at both Lunar Lake and Rogers Lake appear quasi-Lambertian. However, at the Lunar Lake site, as shown in Figure 9, there is a gradual decrease in the HDRF with a viewing angle, in both forward and backward scattering. The HDRF values determined for Rogers Lake in December were generally about 5–10% lower than the values determined in May, when the lake surface was more dry and bright. However, they have similar angular features nonetheless.

The shift of the specular emission angle noticed in Figures 7 and 8, where the peaks in the forward scattering are at angles larger than the Sun zenith angles, has been reported by previous work [*Shepard et al*., 1991] and was qualitatively explained as due to the distribution of the orientations of the slopes of the surface facets. *Ahmad and Deering* [1992] successfully modeled this behavior by combining *Hapke*'s [1981, 1984] approach with *Cox and Munk*'s [1954] formulation to account for the specular reflection from rough surfaces in addition to an empirical term to explain the hot spot phenomenon.

5.3. BRF Results

The BRF values were evaluated using the iterative technique discussed in section 4.2. Each iteration requires the evaluation of $L_t^{r(\mathrm{diff})}$ by computing the integrand in (10) on a grid of zenith and azimuth angles for the incident radiance. The process is repeated to calculate the surface BRF at the viewing and illuminating directions of interest. Gaussian integration technique was used in the computations. For efficiency the computations were made at eight Gaussian integration points in μ and 12 points in $\phi - \phi'$. Error analyses, discussed below, show that eight Gaussian integration points were optimum for combining accuracy and efficiency of the computations.

Calculations were made using the absolute- and relative-radiance approaches discussed above. With the absolute-radiance approach the calibration offset factor g_0 (corrected using the ASD data as explained above) and gain coefficient g_1 were used to convert the PARABOLA digital response (DN) into radiances, according to (3) (g_2 was neglected in these calculations). The exoatmospheric irradiance E_0 was taken from *Wehrli* [1986], and the optical thickness τ, required by this approach, was determined from simultaneous field measure-

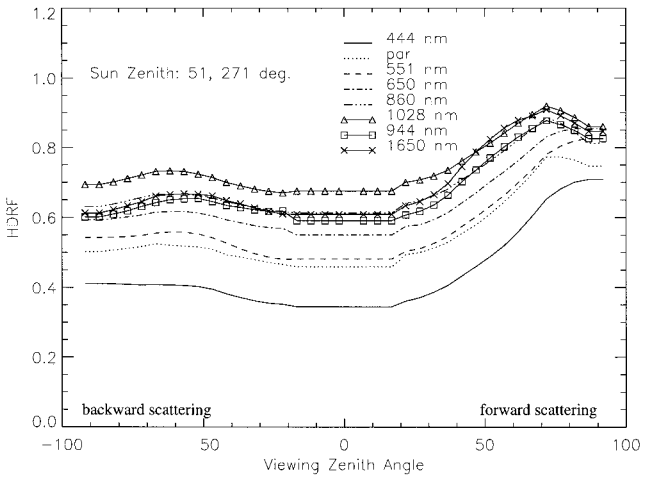

Figure 7. Samples of the surface HDRF results for Lunar Lake on June 24, 1997. The results are presented in the principal plane. As in Figure 6 the HDRF shows a prominent forward scattering ($\phi - \phi_0 = 0$) which peaks at angles larger than the Sun zenith angle. The backward scattering ($\phi - \phi_0 = 180$) is almost uniformly diffuse with slight bumps at longer wavelengths near the Sun zenith angle, indicating weak hot spots.

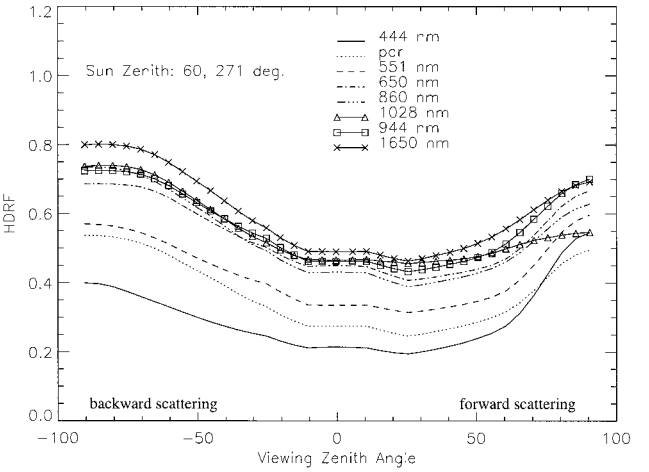

Figure 8. Same as in Figure 7 but for Rogers Lake on May 10, 1998. The surface HDRF exhibits the common bowl shape with the backward scattering becoming more prominent at longer wavelengths.

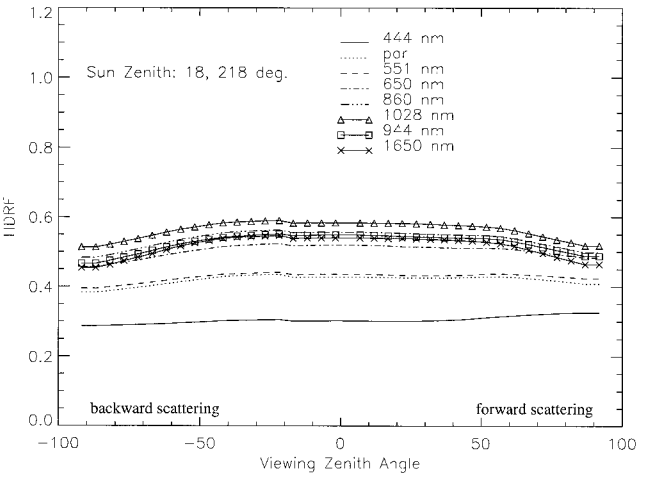

Figure 9. Same as in Figure 7 but near solar noon. The surface is quasi-Lambertian with gradual decrease in the HDRF in both forward and backward scattering at large view angles for the longer wavelengths.

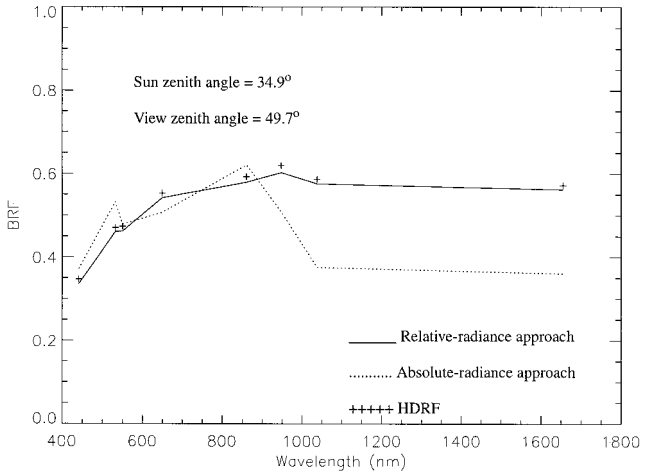

Figure 10. Illustrates the BRF retrieved from the PARABOLA observations at Lunar Lake on June 24, 1997. The disagreement between the two approaches at longer wavelengths is attributed to the uncertainty in the radiometric calibration coefficient g_1 which is required with the absolute-radiance retrieval approach. For comparison the surface HDRF, retrieved for the same illumination and viewing geometry, is also shown.

ments. With the relative-radiance approach, only the corrected offset factor g_0 is required to evaluate the ratio on the right-hand side of (14). In both approaches the process converges after only a few iterations, especially at longer wavelengths. Results from the two approaches, shown in Figure 10 for Lunar Lake, are in reasonable agreement only in the wavelength range corresponding to MISR four channels (446, 558, 672, and 866 nm). The disagreement at larger wavelengths is attributed mostly to the uncertainties in the values of the gain coefficient g_1 due to using laboratory detector standards suitable specifically for MISR channels [*Bruegge et al*., 2000a]. The retrieval of the surface BRF from the PARABOLA observations is best calculated using only the relative-radiance approach.

The surface BRF retrieved for all the three campaigns, using the relative-radiance approach, exhibit the same directional behavior as the corresponding HDRF presented above. The percentage relative difference between the two parameters is within 3–5% for most of the viewing and illuminating geometries. This is expected since the data analyzed here were collected under clear atmospheric conditions. However, these differences increase with Sun and/or viewing angles and at shorter wavelength where diffuse atmospheric scattering becomes relatively more effective. Figure 11 illustrates these differences as a function of wavelength. Samples of the retrieved BRF are presented in Figures 12a and 12b.

6. Error Estimation

The techniques used here to calculate the HDRF and the BRF utilize the ratios of the radiances reflected by the target surface to those reflected by the standard surface, as given by (8) and (14), for the determination of the HDRF and BRF (relative-radiance approach), respectively. As a result, the errors incurred due to uncertainties in the data are greatly diminished.

In the case of the HDRF the sources of errors are the uncertainties in the PARABOLA observations, the value of g_0, and the Spectralon BRF. The latter has been measured in the laboratory with less than 3% error (B2000). The evaluation of g_0, using the ASD results as standard, is sensitive to uncertainties in the ASD and in the PARABOLA observations. The former, from numerous field observations and data analyses, are believed to be known to better than ±1.5%. The uncertainties in the PARABOLA data are mostly due to misalignment, data processing techniques, which use interpolation and smoothing, and noise in the data. The PARABOLA alignment is known to better than ±2°. Errors due to misalignment were evaluated by shifting the data by ±2° and estimating the root mean square of the relative differences between the original and the shifted data. The combined effects of all known sources of errors were evaluated at reflectance levels of 0.1, 0.3, and 0.6. The corresponding errors in the HDRF results were estimated to be about ±7.5, ±5, and ±3%, respectively, for viewing and Sun zenith angles less than 75°. At Sun and viewing zenith angles larger than 75°, these errors almost double.

In the case of the BRF there are additional errors due to the iterative and integration techniques. These errors were evaluated using simulated data. A set of BRF functions, evaluated using a theoretical model, were used in radiative transfer calculations to simulate the PARABOLA observations for the atmospheric conditions existing during the experiments. The simulated data were then used with the retrieval algorithm to evaluate the BRF. The calculations were repeated using 16, 12, and 8 Gaussian integration points. The errors were evaluated by comparing the model calculated (considered the ground truth) with the retrieved BRF. The results using eight Gaussian points were not significantly different from those obtained using 12 or 16 points. This is attributed to the fact that $L_t^{r(\mathrm{diff})}$, evaluated by the Gaussian integration, is only about 20–30% of the total upwelling radiance at the shorter wavelengths and about 10% or less for the longer wavelengths. The effects of the above sources of uncertainties were also evaluated at reflectance level of 0.1, 0.3, and 0.6. The corresponding uncertainties in the BRF, retrieved using the relative-radiance approach, were found to be about ±8, ±4.5, and ±3.5%,

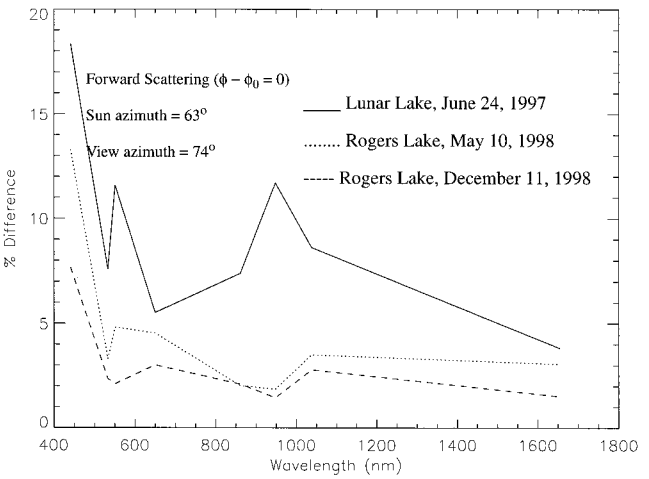

Figure 11. Percentage relative difference between surface HDRF and BRF as a function of wavelength, for the three PARABOLA experiments. The difference increases with view and Sun angles and is maximum at 444 nm.

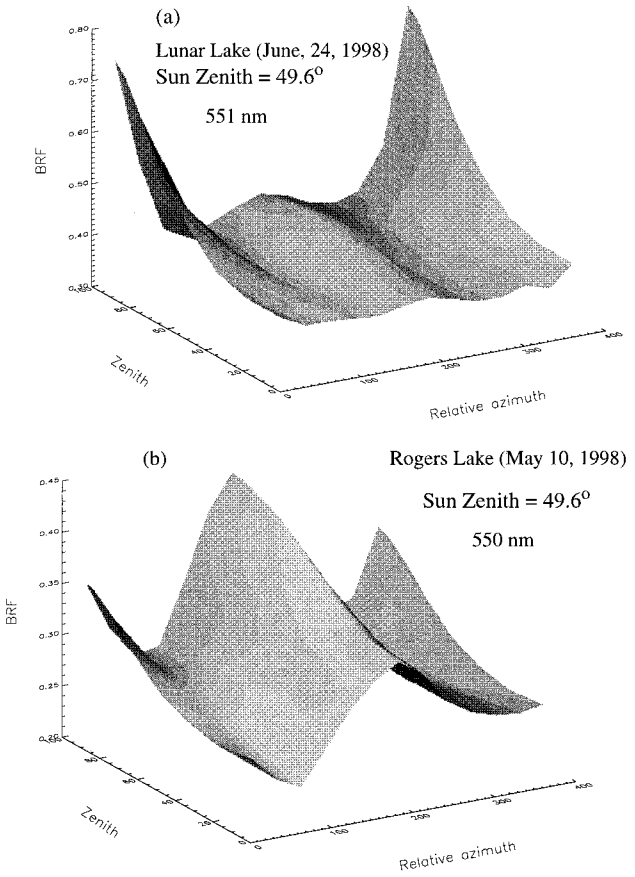

Figure 12. Samples of the surface BRF retrieved for (a) Lunar Lake and (b) Rogers Lake, shown as functions of the view zenith and azimuth angles (the latter relative to the Sun). The surface BRF behaves similar to the HDRF, exhibiting stronger forward scattering (relative azimuth = 0) at Lunar Lake and stronger backward scattering (relative azimuth = 180°) at Rogers Lake. The shades of gray in this figure are automatically generated by the plotting routine and have no quantitative values.

respectively. For the absolute-radiance approach the errors are very sensitive to uncertainties in the calibration coefficients g_0 and g_1. Until these are known to better than $\pm 3\%$, the BRF is best retrieved using the relative-radiance approach. However, assuming these coefficients and the optical depth are measured to better than $\pm 3\%$, the errors in retrieving the BRF using the absolute-radiance approach are similar to those evaluated for the relative-radiance approach.

7. Summary

The PARABOLA 3 instrument is a multiangle sphere-scanning radiometer that provides directional observations of sky and surface radiances. These observations are suited to retrieving directional reflectance properties of natural surfaces. Ground observations made with the PARABOLA 3 at two dry lake sites were presented, and two algorithms to retrieve the surface BRF and HDRF from these observations were described. The first requires simultaneous measurements of the atmospheric optical depth. The second utilizes the ratios of the radiances reflected by the target surface to those reflected by a standard reference surface. The HDRF is retrieved directly from these ratios, while the BRF retrieval requires the removal of the diffuse component from the observed radiances. Using the second approach, the surface BRF and HDRF were retrieved within ± 8, ± 4.5, and $\pm 3.5\%$ at reflectance levels of 0.1, 0.3, and 0.6, respectively, for Sun and viewing zenith angles less than 75°. These errors almost double at larger angles. The data described here are used, with other simultaneous field measurements, for the validation and vicarious calibration of MISR and AirMISR, as described by *Abdou et al*. [2000].

Acknowledgment. The work presented here was conducted at the Jet Propulsion Laboratory, California Institute of Technology, under contract with the National Aeronautics and Space Administration.

References

Abdou, W. A., J. E. Conel, S. H. Pilorz, M. C. Helmlinger, C. Bruegge, and B. J. Gaitley, Vicarious calibration: A reflectance-based experiment with AirMISR, *Remote Sens. Environ*., in press, 2000.

Ahmad, S. P., and D. W. Deering, The role of specular reflectance in surface anisotropy, IGARSS'92, *Int. Geosci. Remote Sens. Symp*., pp. 514–516, 1992.

Bruegge, C. J., M. C. Helmlinger, J. E. Conel, B. J. Gaitley, and W. A. Abdou, PARABOLA III: A sphere-scanning radiometer for field determination of surface anisotropic reflectance functions, *Remote Sens. Rev*., in press, 2000a.

Bruegge, C. J., J. V. Martonchik, and A. H. Strahler, A review of reflectance nomenclature used in remote sensing, *Remote Sens. Rev*., in press, 2000b.

Charney, J., W. J. Quirk, S. Chow, and J. Kornfield, A comparative study of the effects of albedo change on drought in semi-arid regions, *J. Atmos. Sci*., *34*, 1366–1385, 1977.

Cox, C., and W. H. Munk, The measurements of the roughness of the sea surface from photographs of the sun glitter, *J. Opt. Soc. Am*., *44*, 838–850, 1954.

Deering, D. W., Parabola directional field radiometer for aiding in space sensor data interpretations, *Proc. SPIE Int. Soc. Opt. Eng*., *924*, 249–261, 1988.

Deering, D. W., and P. Leone, A sphere-scanning radiometer for rapid directional measurements of sky and ground radiance, *Remote Sens. Environ*., *19*, 1–24, 1986.

Dickinson, R. E., B. Pinty, and M. M. Verstraete, Relating surface albedos in GCM to remotely sensed data, *Agric. For. Meteorol*., *52*, 109–131, 1990.

Diner, D. J., et al., Multiangle Imaging Spectroradiometer (MISR) description and experiment overview, *IEEE Trans. Geosci. Remote Sens*., *36*, 1072–1087, 1998a.

Diner, D. J., et al., The Airborne Multiangle Spectroradiometer (AirMISR): Instrument description and first results, *IEEE Trans. Geosci. Remote Sens*., *36*, 1339–1349, 1998b.

Hapke, B., Bidirectional reflectance spectroscopy, 1, Theory, *J. Geophys. Res*., *86*, 3039–3054, 1981.

Hapke, B., Bidirectional reflectance spectroscopy, 3, Correction for macroscopic roughness, *Icarus*, *59*, 41–59, 1984.

Irons, J. R., K. J. Ranson, D. L. Williams, R. R. Irish, and F. G. Huegel, An off-nadir pointing imaging spectroradiometer for terrestrial ecosystem studies, *IEEE Trans. Geosci. Remote Sens*., *29*, 66–74, 1991.

Liang, S., and A. H. Strahler, An analytic BRDF model of canopy radiative transfer and its inversion, *IEEE Trans. Geosci. Remote Sens*., *31*, 1081–1092, 1993.

Liang, S., and A. H. Strahler, Retrieval of surface BRDF from multiangle remotely sensed data, *Remote Sens. Environ*., *50*, 18–30, 1994.

Martonchik, J. V., Retrieval of surface directional reflectance properties using ground level multi-angle measurements, *Remote Sens. Environ*., *50*, 303–316, 1994.

Martonchik, J. V., D. J. Diner, B. Pinty, M. M. Verstraete, R. B. Myneni, Y. Knyazikhin, and H. R. Gordon, Determination of land and ocean reflective, radiative and biophysical properties using multi-angle imaging, *IEEE Trans. Geosci. Remote Sens*., *36*, 1266–1281, 1998.

Mintz, Y., *The Global Climate*, edited by J. T. Houghton, pp. 79–105, Cambridge Univ. Press, New York, 1984.

Nicodemus, F. E., J. C. Richmond, J. J. Hsia, I. W. Ginsberg, and T. Limperis, Geometrical considerations and nomenclature for reflectance, *NBS Monogr. 160*, Natl. Bur. of Stand. U.S. Dep. of Comm., Washington, D. C., 1977.

O'Neill, N. T., J. R. Miller, and J. R. Freemantle, Atmospheric correction of airborne BRF to yield surface BRF: Nomenclature, theory, and methods, *Can. J. Remote Sens*., *21*(3), 1995.

Pinty, B., and M. M. Verstraete, On the design and validation of surface bidirectional reflectance and albedo models, *Remote Sens. Environ*., *41*, 155–167, 1992.

Pinty, B., M. M. Verstraete, and R. E. Dickenson, A physical model for predicting bidirectional reflectance over bare soils, *Remote Sens. Environ*., *27*, 273–288, 1989.

Shepard, M. K., R. E. Arvidson, E. A. Guinness, and D. W. Deering, Scattering behavior of Lunar Lake Playa determined from PARABOLA bidirectional reflectance data, *Geophys. Res. Lett*., *18*(12), 2241–2244, 1991.

Wehrli, C., Extraterrestrial solar spectrum, *WCRP*, *Publ. Ser. 7*, *WMO ITD-149*, pp. 119–126, World Clim. Res. Program, World Meteorol. Organ., Geneva, Switzerland, 1986.

Verstraete, M. M., B. Pinty, and R. E. Dickinson, A physical model of the bidirectional reflectance of vegetation canopies, 1, Theory, *J. Geophys. Res*., *95*, 11,755–11,765, 1990.

W. A. Abdou, C. J. Bruegge, J. E. Conel, B. J. Gaitley, M. C. Helmlinger, J. V. Martonchik, and S. H. Pilorz, Jet Propulsion Laboratory, California Institute of Technology, 4800 Oak Grove Drive, Pasadena, CA 91109. (wedad.a.abdou@jpl.nasa.gov)

(Received April 29, 2000; revised September 12, 2000; accepted September 19, 2000.)